

## Disk evolution of the M87's nucleus observed in 2008

Fei Xiang<sup>1</sup> and Cheng Cheng<sup>2</sup>

<sup>1</sup> Department of Astronomy, Yunnan University, Kunming 650091, China, [xiangf@ynu.edu.cn](mailto:xiangf@ynu.edu.cn)

<sup>2</sup> Chinese Academy of Sciences South America Center for Astronomy, National Astronomical Observatories, CAS, Beijing 100101, China, [chengcheng@bao.ac.cn](mailto:chengcheng@bao.ac.cn)

Received 20xx month day; accepted 20xx month day

**Abstract** We report the discovery of year-scale X-ray variation in the nuclear region of the M87 by reanalyze the 8 Chandra observations from 2007 to 2008. The X-ray spectra are fitted and decomposed into disk and flaring components. This year-scale X-ray variability can be explained quite well by a simple clumpy accretion model. We conclude that the central super-massive blackhole of the M87 was accreting a cloud of  $\sim 0.5M_{\odot}$  at that time.

**Key words:** galaxies:active–X-ray:individual:M87

### 1 INTRODUCTION

The nucleus of M87 galaxy is an ideal object for studying gas accretion into central Super-Massive Black Hole(SMBH). The proximity ( $\sim 16$  Mpc) of M87 makes its central tens-parsec region resolvable in various wavelength (e.g., Optic: Perlman et al. 1999, radio: Biretta et al. 1995, x-ray: Marshall et al. 2002). Based on the *Chandra* observations, Di Matteo et al. (2003) obtained that the mass accretion rate ( $\dot{m}$ ) is  $\sim 10^{-3}$  of Eddington accretion rate ( $\dot{m}_{\text{Edd}}$ ) and the radiation efficiency ( $\eta$ ) is  $\sim 10^{-5}$ . Recently, Levinson & Rieger (2011) suggested that the ratio of  $\dot{m}$  over  $\dot{m}_{\text{Edd}}$  should be as low as  $\sim 10^{-4}$ . These observations implied that the central region of M87 is under the Radiation Inefficiency Accretion Flow (RIAF) mode.

The Advection Dominated Accretion Flow (ADAF, Narayan & Yi 1994) model, the most widely applied RIAF model, has successfully explained the emission from Low Luminosity AGNs (LLAGNs) and been applied to M87 (Ho 2008, Nemmen et al. 2014, see Yuan & Narayan 2014 for a detail review). By analysis of the Spectral Energy Distribution (SED), it was found that the X-ray emission from M87's nucleus could be mainly attributed to ADAF component (Di Matteo et al. 2003, Wang et al. 2008, Li et al. 2009, Cui et al. 2012, Nemmen et al. 2014).

For the LLAGNs, one of the interesting issues is the evolution of the accretion mode. Theoretical models have proposed that the gas flow in LLAGNs might be clumpy, which could lead to some year-scale variation in mass accretion rate (Yuan 2003, Wang et al. 2012). The variation of mass accretion rate could be detected through the variation of X-ray luminosity, provided the bolometric luminosity of pure ADAF can be estimated by X-ray luminosity multiplying a bolometric correction (Elvis et al. 1994, Ho 1999, Hopkins et al. 2007). The year-scale variation of X-ray flux has been found in M81 with Swift/XRT (Pian et al. 2010). Considering the similarity of LLAGNs and the larger scale of the M87's accretion flow, it can be expected that such variation might be found in M87, which might give some constraints on inhomogeneous accretion model.

*Chandra* observations have revealed month-scale variations of the nuclear X-ray luminosity in M87 (Harris et al. 2009), which may be accompanied by the change of the X-ray spectrum (Hilburn

& Liang 2012). Although the X-ray emission in the ‘low state’ (i.e. low luminosity) of M87 can be explained by pure ADAF model (Di Matteo et al. 2003, Wang et al. 2008, Li et al. 2009). The X-ray emission in ‘high state’ (i.e. high luminosity) might have more complex components and behaviors due to the occasion of the mini-jet (Giannios et al. 2010, Cui et al. 2012). Thus, it is necessary to check the X-ray contents of ‘high state’ carefully.

In addition, M87 is the unique non-blazar radio galaxy detected to emit Very High Energy (VHE) gamma rays. In Feb 2008, a giant VHE flare was observed in M87 by MAGIC and VERITAS respectively (Albert et al. 2008, Acciari et al. 2009). Subsequently, a *Chandra* observation to M87’s nucleus was performed 3 days after the VHE flare and a sharp enhancement in the nuclear X-ray luminosity was observed, indicating that the location of the VHE flare was in the M87’s nucleus (Harris et al. 2009). In 2010, another VHE flare was captured. With the help of subsequent multi-wavelength observations (VHE: VERITAS, MAGIC, H.E.S.S; X-ray: Chandra; radio: 43GHz, VLBA; Aliu et al. 2012, Abramowski et al. 2012, Hada et al. 2012), the location of the flare was confirmed to be near the black-hole, which suggests that the VHE and X-ray flares come from the outburst near the SMBH (Cui et al. 2012). This succeeding variability in  $\gamma$ -ray and x-ray bands might offer us more hints about the evolution of nucleus in M87.

In this paper, We re-analyze a series of *Chandra* observations from July 2007 to August 2008 (PI: Dr. John Biretta) and find a year-scale variability component which could be explained by a simple inhomogeneous accretion model. This paper is arranged as follows, data analysis is described in section 2, the spectra fitting results are presented in section 3, the clumpy accretion and the contents of X-ray emission are discussed in section 4 and finally the conclusions come in Section 5.

## 2 DATA ANALYSIS

From 2007 to 2008, eight *Chandra* observations to M87 (Observation ID: from 7354 to 8581) were proposed by Dr. John Biretta, aimed to monitor the HST-1 and revealed nuclear X-ray brightening after the VHE flare (Harris et al. 2009). The HST-1 is a knot in M87’s jet. It was revealed by the HST (Boksenberg et al. 1992) and draw the attention from x-ray to radio band soon after the discovery. The HST-1 is much brighter than the nucleus and shows strong variability in X-ray. Its X-ray luminosity had been increasing from 2001 to 2005 and started to decrease after 2005. Its peak luminosity in 2005 could reach about 10 times of the nuclear luminosity. Because the location of HST-1 is near the nucleus (65 pc projected), it may produce the ‘light pollution’ on nucleus (Harris et al. 2003, 2006, 2009). To avoid strong ‘light pollution’, we choose the data from 2007 to 2008 for analysis. At that time, the HST-1’s x-ray luminosity became comparable to that of nucleus. The possible ‘light pollution’ from HST-1 will be discussed in later paragraphs. The livetime for each observation is about 4.7 ks, the observation instrument is ACIS-I, and the observation mode is FAINT. Under the FANIT mode, the frametime is 0.4 s to avoid the significant pileup effect. Even for the brightest observation (ID: 8577), the peak counts rate of the nucleus is  $\sim 0.2$  counts  $s^{-1}$  pixel $^{-1}$ . The counts rate per frame is  $\sim 0.08$  counts  $s^{-1}$ . At this level, the pileup fraction is less than 5% (Davis 2001). The peak counts rates of the other observations are around 0.1 counts  $s^{-1}$  pixel $^{-1}$ . So the following spectral fittings is free of the pileup effect.

In our analysis, The level 2 data is processed with CIAO 4.2 and CALDB 4.2.0, which is produced through the Standard Data Processing (SDP), in which good time intervals (GTIs) filtering, cosmic ray rejection, and position transformation are performed. The structure of nucleus and jet is clear in the images of these observations (e.g. ID: 8576 at Jan. 4th 2008 in Fig 1). The center of the X-ray nucleus is located at R.A.=  $12^{\text{h}}30^{\text{m}}49^{\text{s}}.42$ , Dec.=  $12^{\circ}23'28''.05$  (J2000) which is consistent with that of previous observations (Wilson & Yang 2002). To extract the spectra of nucleus, we select the box region including nucleus ( $1''.8 \times 2''.3$ ) as the source region for every observation (Fig 1). The location of source regions are chosen on the basis of contours (e.g. bottom panel in Fig 1). To eliminate the contribution of foreground and background, we select a box region beside the source ( $17''.0 \times 8''.5$ ) as the background region (top panel in Fig 1), where no clear point source has been detected. The spectra, Ancillary Response Files (ARFs) and Response Matrix Files (RMFs) are generated through the ‘speextract’ script in CIAO. The size of source region is comparable to the size of Point-Spread Function (PSF).

Table 1: The parameters of spectra fitting with absorbed power law. The error bars are calculated with the confidence of 68%

ID	Photon index	norm ( $10^{-5}$ )	flux <sub>2-10keV</sub> ( $10^{-12}$ erg/s/cm <sup>2</sup> )	$\chi^2$ /DOF
7354	$2.29 \pm 0.07$	$39 \pm 2$	$0.66 \pm 0.06$	12.58/27
8575	$2.02 \pm 0.05$	$69 \pm 2$	$1.70 \pm 0.10$	40.53/37
8576	$2.10 \pm 0.05$	$74 \pm 2$	$1.62 \pm 0.12$	37.69/40
8577	$1.71 \pm 0.03$	$119 \pm 3$	$4.74 \pm 0.20$	63.83/65
8578	$1.78 \pm 0.04$	$74 \pm 2$	$2.68 \pm 0.14$	49.29/46
8579	$2.12 \pm 0.05$	$69 \pm 2$	$1.47 \pm 0.10$	36.56/37
8580	$1.75 \pm 0.04$	$91 \pm 2$	$3.38 \pm 0.15$	59.13/55
8581	$2.15 \pm 0.05$	$57 \pm 2$	$1.16 \pm 0.08$	69.01/74

The ‘arccorr’, which is performed automatically in ‘specextract’ script, will give the correction factors on ARFs. In corrected ARFs, the column ‘PSF FRACTION’ presents the fraction of PSF counts within the selected region at each energy band (<http://xc.harvard.edu/ciao/threads/pointlike/>). We checked the PSF Fraction in every corrected ARFs, ensuring the PSF Fraction is from 0.85 (hard band) to 0.95 (soft band). The contribution of adjacent HST-1 has been estimated to be about 6% by Harris et al. (2006).

### 3 RESULTS

Previous observations to M87’s nucleus indicate that the nuclear X-ray spectra could be fitted well with an absorption-modified powerlaw model (Wilson & Yang 2002). So we use XSPEC (version 12.6.0) to fit the spectra with the model as follows (Arnaud 1996):

$$Model_1 = Wabs(n_H) \times Powerlaw(\Gamma, norm) \quad (1)$$

The equivalent hydrogen column density ( $n_H$ ) is fixed as  $\sim 6.1 \times 10^{20} \text{cm}^{-2}$  in the spectra fitting of this work, which is derived by Wilson & Yang (2002). The resulting photon index, normalization of the spectra and flux (2-10keV) are given in Table 1. The spectral variations are shown in Fig 2, which reveals a month-scale variability. The nuclear luminosity increases sharply and then returns to the original level in a scale of month with the photon index changing in reverse direction.

The 2-10keV luminosity light curve in Fig 2 is consistent with the photometric light curve obtained by Harris et al. (2009). The Fig 3 illustrates the relation between the photon index ( $\Gamma$ ) and flux, from which we could divide the states of nucleus into two types. The five observations with the photon index about 2.1 and low flux are denoted as the ‘first class’, which are shown by triangles in Fig 3; the rest three observations with the photon index around 1.75 and relatively high flux are denoted as the ‘second class’ (dots in Fig 3).

For the first class, the previous studies have confirmed that their SED could be explained by pure ADAF model (Di Matteo et al. 2003, Li et al. 2009, Cui et al. 2012). And the latest SED fitting by the model of ADAF plus jet also suggests that ADAF component dominates the X-ray emission (Nemmen et al. 2014). In addition, recent studies of polarization show that the optical polarization of the nucleus is much lower than that of HST-1 in M87, which implies that the radiative mechanism of the nucleus may be different from the HST-1’s (Perlman et al. 2011, Adams et al. 2012). Based on these results, it is likely that the X-ray emission of the first class is mainly attributed to the ADAF component. For the second class, the X-ray spectra become harder with the increasing of flux. In the observation of 02/16/2008, X-ray luminosity brightened up after the VHE flare. So it is plausible that the flares occurred in these observations. We could induce that there are two components in their X-ray emission: one is the flaring component and the other is the quiescent component whose spectrum is similar to that of the first class.

The variations of the X-ray emission in M87 nucleus also can be divided into two types (Fig 2, Fig 5). Firstly, the flares occur in the scale of month and are corresponding to the spectra changing from the first class to the second class. Secondly, the nuclear luminosity of the first class exhibits a year-scale

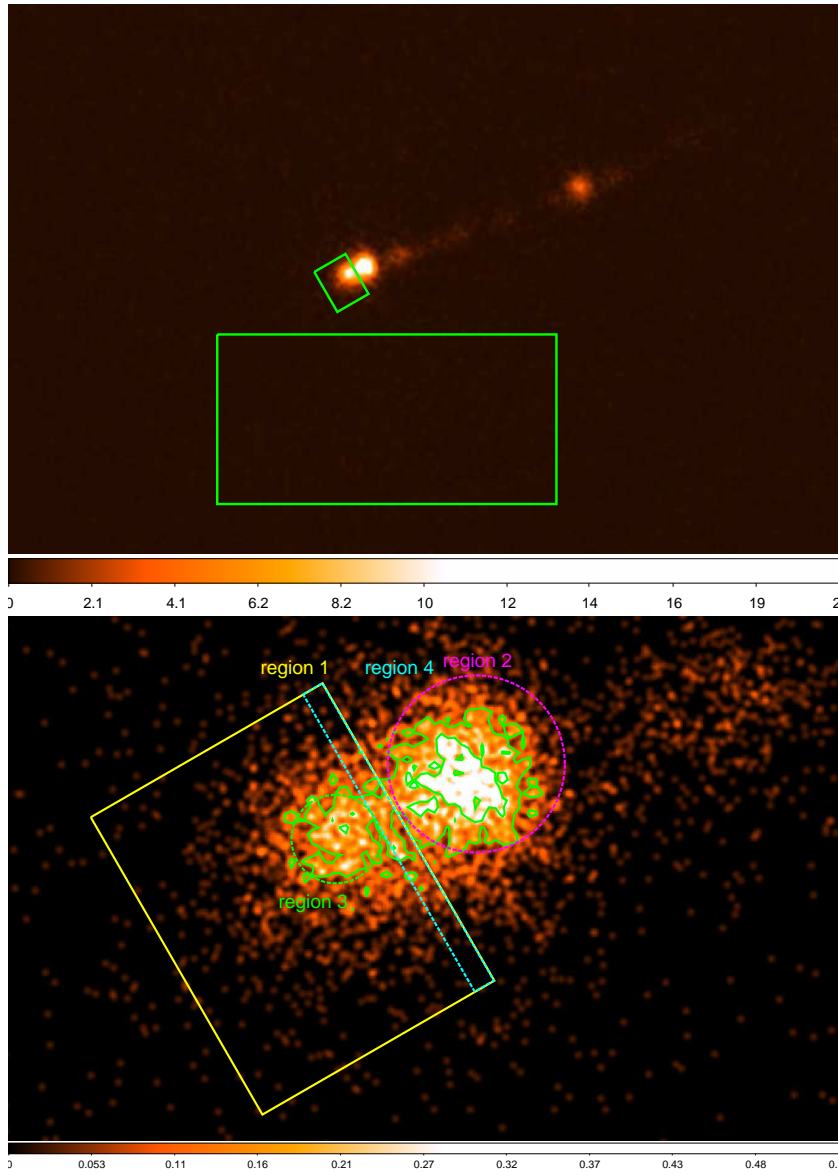


Fig. 1: The X-ray image of M87's jet observed on Jan 4th 2008. In top panel, the small box indicate the source region and the big box is the background region; the left point source is the nucleus and the right point source is the HST-1. Bottom panel shows that the box of the source region is chosen on the basis of contours. The contour levels are 0.12, 0.24 and 0.48 counts per bin. Bin size is pixel/64 and a Gaussian smoothing with kernel radius of 5 bins is applied. In bottom panel, yellow solid box: source region (region 1); magenta dotted circle: HST-1 (region 2); green dotted circle: nucleus' center (region 3); cyan dotted strip: region between nucleus' center and HST-1 (region 4).

evolution (triangles in Fig 5), which shows the trend of fast rising ( $\sim 4.2 \times 10^{40}$  erg/s,  $10\sigma$ ) in 4 months and then slow fading ( $\sim 2.2 \times 10^{40}$  erg/s,  $5\sigma$ ) in about 8 months. We have checked the variability of the first class in Fig 5 through reduced Chi-square test. For all five points, the probability (P value) of no variation is less than  $10^{-5}$ . So it could be affirmed that the year-scale evolution of X-ray emission

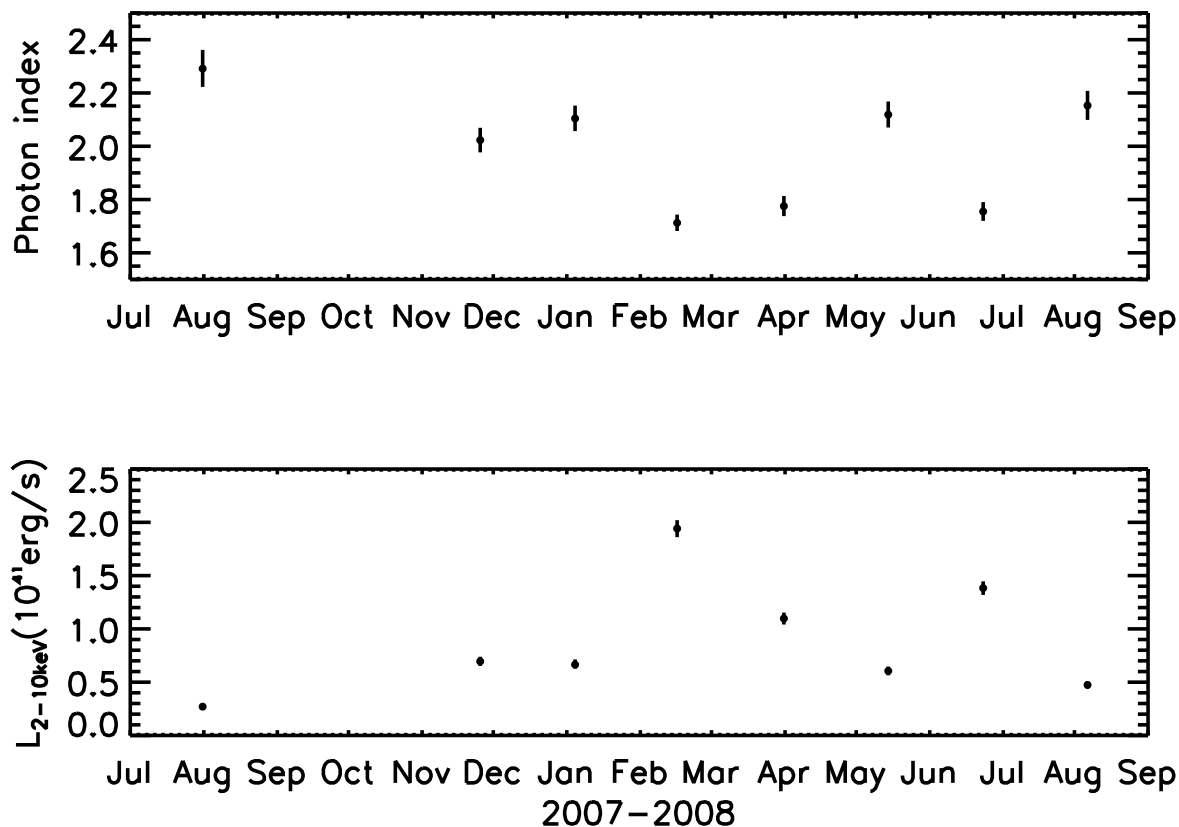


Fig. 2: The variation of the X-ray spectra parameters observed in M87's nucleus from July 2007 to September 2008.

exists in M87. Considering the complexity of the second class, we only consider the results of the first class when investigating the evolution of ADAF content (triangles in Fig 5).

In our analysis, the  $n_{\text{H}}$  is fixed as  $6.1 \times 10^{20} \text{ cm}^{-2}$ . The range of  $n_{\text{H}}$  given by Wilson & Yang (2002) is  $4.7 \sim 7.6 \times 10^{20} \text{ cm}^{-2}$  (90% confidence), showing an excess above the Galactic value ( $2.5 \times 10^{20} \text{ cm}^{-2}$ , Stark et al. 1992). But Harris et al. (2006) demonstrate that the derived  $n_{\text{H}}$  highly depends on the fitting model. To demonstrate the impact of the uncertainty in  $n_{\text{H}}$ , we change the  $n_{\text{H}}$  in fitting from  $2.5 \times 10^{20}$  to  $8.5 \times 10^{20} \text{ cm}^{-2}$ . The reduced  $\chi^2$  of these fittings are still acceptable ( $\leq 1.1$ ). The variation of  $n_{\text{H}}$  could cause a change of  $\pm 6\%$  on the derived flux and  $\pm 0.1$  on the photon index. The uncertainty in  $n_{\text{H}}$  may blur the difference of photon index between the first and the second class. But the variation of  $n_{\text{H}}$  can only produce the variation of  $\pm 6\%$  on luminosity and can not explain the luminosity evolution observed in the first class. Provided that we still use the same  $n_{\text{H}}$  in 8 spectra fittings, our conclusion will not be apparently affected.

Another factor to be taken into account is the ‘light pollution’ of HST-1. Firstly, the source regions in data analysis are chosen on the basis of contours. In the 5 observations when the nucleus is bright (ObsID: 8575, 8576, 8577, 8578, 8580), the separation of contours is clear but there still is about 6% of the light counts that come from HST-1 (Harris et al. 2006). For the 3 observations in which the emission of nucleus is weak (ObsID: 7354, 8579, 8581), the boundary is blurry so that the source regions may include larger fraction of counts from HST-1 than the 5 other observations. In this case, the actual nuclear emission in these 3 observations may be weaker and the year-scale variation may be more intense than what has been observed. Secondly, the detections of nucleus and HST-1 may suffer from a mutual effect of pileup called ‘Eat Thy Neighbor’ (Harris et al. 2006, 2009). When two photons from

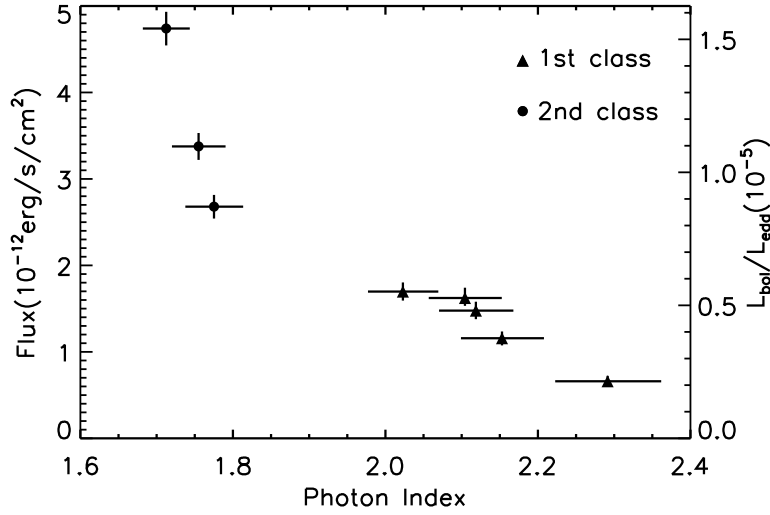


Fig. 3: The relation between the X-ray photon index and the flux. The  $L_{\text{Bol}}$  is calculated by  $L_{\text{Bol}}/L_{2-10\text{keV}} \sim 30$  (Elvis et al. 1994, Hopkins et al. 2007) and the  $L_{\text{Edd}}$  is calculated with the black hole mass of  $3 \times 10^9 M_{\odot}$  (Fabian & Rees 1995, Macchetto et al. 1997).

each other come within  $3 \times 3$  pixel grid at the same frame, they will be considered as one event and the event position is determined by the harder photon. If HST-1 become brighter, the nuclear emission will be eaten more. As result, we can only choose the observations in which HST-1 is not so bright for analysis. Finally, if pileup is significant, it will distort the PSF, which is called “second-order effect of pileup” in Harris et al. (2009). The second order effect is hard to be estimated. A possible way of reducing this effect is to select the observations in which the pileup effect is not too strong for nucleus and HST-1.

Because the complexity for estimating the contamination directly, to determine the influence of HST-1 to our results, we check the correlation of light curves between different regions with the HST-1. We choose four regions to derive the counts rate light curve. The first region is rectangle source region (region 1,  $1''.8 \times 2''.3$ ); the second region is the circle region at HST-1 (region 2, radius:  $0.6''$ ); the third region is the circle region at nucleus' center (region 3, radius:  $0.3''$ ); the fourth region is the strip region between HST-1 and nucleus' center (region 4,  $0''.15 \times 2''.3$ ) (Fig 1). The light curves of the four regions are shown in Fig 4. We found that the light curve of region 2 (HST-1) has an opposite trend with those of region 1 (source region) and region 3 (central nucleus). Their correlation coefficient is  $-0.56$ , which is similar with the Harris et al. 2009's result. The light curves of region 1 and region 3 have the same trend and the correlation coefficient is  $0.99$ . The region 4 (strip region) is the region which may subject to the 'light pollution' most possibly. But in Fig 4, its counts rate changes slightly. Its correlation coefficient with HST-1 is  $-0.45$  and that with the nucleus is  $0.81$ . The above correlation coefficients suggest that change of the source region is determined by the nucleus and the strip region is influenced by HST-1 little.

Further, if we assume that the counts rate of strip region is influenced by HST-1 and the nucleus simultaneously, the counts rate of the region 4 could be expressed as  $Z = A * X + B * Y + C$ : the  $X, Y, Z$  are the counts rate of region 2, 3, 4 respectively and  $A, B, C$  are the constants. We could conduct a multivariate fitting to above light curves. We derive  $A, B$  and  $C$ 's values:  $0.0002, 0.1$  and  $0.033$ . The very low value of coefficient  $A$  indicates little influence from HST-1, which confirms the above conclusion.

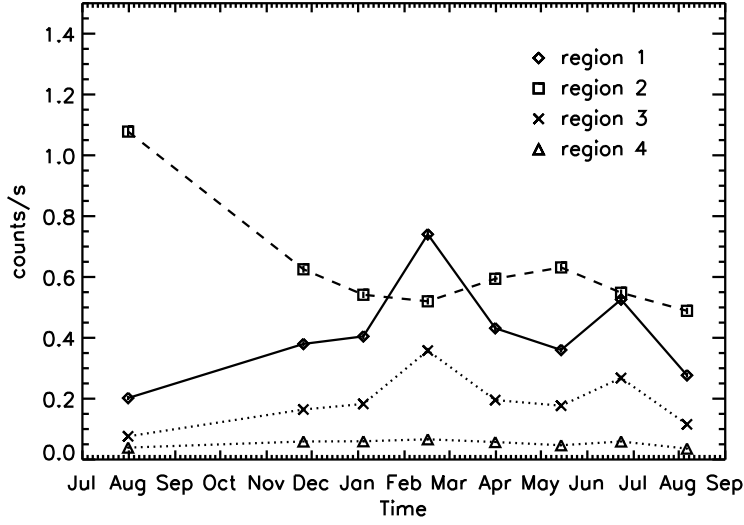


Fig. 4: The light curves of the above four regions.(Diamond: region 1; Square: region 2; Cross: region 3; Triangle: region 4.)

## 4 DISCUSSION

### 4.1 Clumpy accretion in M87

For the first class (quiescent state), the nuclear luminosity shows a slow evolution within a year (triangles in Fig 5). For all five points, the disk luminosity was the lowest in the observation made on 07/31/2007 and then increased quickly to the highest in early 2008, reaching  $\sim 7.0 \times 10^{40}$  erg/s (the increment  $\sim 10\sigma$ ). After that, in observation of late 2008, the nuclear luminosity decreased to  $\sim 4.7 \times 10^{40}$  erg/s slowly (the decrement  $\sim 5\sigma$ ). We define the mass accretion rate as  $\dot{m} = L_x/(\eta c^2)$ , where  $\eta$  is the X-ray radiation efficiency. Di Matteo et al. (2003) estimate that the average mass accretion rate of M87 is  $\sim 0.1 M_\odot/\text{yr}$  and  $\eta$  is about  $10^{-5}$  through detailed study on the hot interstellar medium in M87. Based on these results, the above variation of X-ray luminosity could be attributed to the variation of mass accretion rate ( $\dot{m}$ ).

The inhomogeneous accretion flow, which is called clumpy accretion, might account for such variability. The gas clumps (clouds), originated from gravitational or thermal instability in accretion flow, might lead to a modulation in luminosity (Ishibashi & Courvoisier 2009, Strubbe & Quataert 2009, Wang et al. 2012). When a clump falls toward the central black hole, it will be disturbed by the tidal force and form a gas ring of high density. Basic equation for such an accretion ring is

$$\frac{\partial \Sigma}{\partial t} = \frac{3}{R} \frac{\partial}{\partial R} \left( R^{1/2} \frac{\partial \nu \Sigma R^{1/2}}{\partial R} \right), \quad (2)$$

with initial matter distribution is:

$$\Sigma(x, \tau = 0) = \Sigma_0 \delta(R - R_0), \quad (3)$$

here  $\Sigma$  is the surface density of the accretion flow,  $R$  is the radius, and  $\nu$  is kinematic viscosity parameter (Lin & Pringle 1987).  $\Sigma_0$  is the initial surface density of the accretion ring and the  $R_0$  is the radius where the ring forms. The  $x = R/R_0$  presents the dimensionless distance to central black hole and  $\tau = (t - t_0)/\tau_0$  where the  $t_0$  is the date when the clumpy accretion started and  $\tau_0$  is time scale of gas falling. For simplicity, we take  $\nu$  as a constant, and thus analytical solution to Equation 5 can be written as(Frank et al. 2002):

$$\Sigma(x, \tau) = \sigma_0 \frac{1}{\tau} \frac{1}{x^{1/4}} e^{-\frac{1+x^2}{\tau}} I_{1/4} \left( \frac{2x}{\tau} \right), \quad (4)$$

and

$$\tau_0 = \frac{R_0^2}{12\nu} \quad (5)$$

Here  $I_{1/4}$  is the modified Bessel function. The falling velocity  $v_R$  could be derived through:

$$v_R = \frac{3}{\Sigma R^{1/2}} \frac{\partial}{\partial R} (\nu \Sigma R^{1/2}). \quad (6)$$

So

$$v_R = -\frac{3\nu}{R_0} \frac{\partial}{\partial R} \left[ \frac{1}{4} - \frac{1+x^2}{\tau} + \ln I_{1/4} \left( \frac{2x}{\tau} \right) \right], \quad (7)$$

asymptotically, the radial velocity is

$$v_R \simeq -\frac{3\nu}{R_0} \left( \frac{1}{2x} - \frac{2x}{\tau} \right) \quad \text{for } 2x \ll \tau, \quad (8)$$

and thus the mass accretion rate for the accretion ring  $\dot{m} = -2\pi R v_R \Sigma$  could be written as:

$$\dot{m}(x, \tau) = \dot{m}_0 \left( \frac{1}{2x} - \frac{2x}{\tau} \right) \frac{x^{3/4}}{\tau} e^{-\frac{1+x^2}{\tau}} I_{1/4} \left( \frac{2x}{\tau} \right), \quad (9)$$

where  $\dot{m}_0 = 6\pi\nu\Sigma_0$ . This solution has the characteristic of "fast rising" and "slow falling", which is similar to the observed X-ray light curve. Fig 5 shows that it could fit well the observational data. The fitting parameters:  $\dot{m}_0 = 0.3 M_\odot \text{yr}^{-1}$ ,  $x = 0.04$ ,  $\tau_0 = 164$  days and  $t_0$  is the 7th June of 2007.  $x = R/R_0 = 0.04$  indicates that the accretion rate obtained here represents the mass accretion rate near the black hole. As shown above, the simple clumpy accretion could produce the year-scale variation of the X-ray luminosity observed in M87's nucleus. The mass of gas clump  $M_c \sim 0.5 M_\odot$  could be obtained through integration of  $\dot{m}$  by time. According to Wang et al. (2012),  $R_0$  should be  $100R_{\text{Sch}} \sim 1000R_{\text{Sch}}$ . and typical density in gas clump ( $n_{\text{cl}}$ ) is  $\sim 10^{14}/\text{cm}^3$ . so we could estimate the radius of clump  $R_c = (3M_c/(4\pi n_{\text{cl}} m_p))^{1/3} \sim 1.13 \times 10^{14}$  cm (here  $m_p$  is the mass of proton).

The anti-correlation of photon index and Eddington ratio in Fig 3 is also a prediction of the ADAF model (Yuan et al. 2007, Gu & Cao 2009). In ADAF, X-ray emission is mainly produced by the Comptonization of hot gas, as described in Gu & Cao (2009), the X-ray's photon index could be calculated by:

$$\Gamma = -\ln \tau_{\text{es}} / \ln A, \quad (10)$$

here,  $\tau_{\text{es}}$  is the electron scattering optical length and could be expressed as  $\tau_{\text{es}} = 24\alpha^{-1}\dot{m}r^{-\frac{1}{2}}$  ( $\alpha$  is the viscosity parameter  $\sim 0.1$ ,  $\dot{m}$  is the accretion rate in unit of Eddington rate, and the  $r$  is the radius in Schwarzschild radii).  $A = 16(k_B T_e / m_e c^2)^2$ , is the mean amplification factor of the photon energy by Comptonization ( $T_e$  and  $m_e$  is the temperature and mass of the hot electrons in ADAF disk) (Rybicki & Lightman 1979). So the photon index  $\Gamma$  is anti-correlated with  $\dot{m}$ . According to Equation 8,  $\Gamma$  is determined by  $\dot{m}$ ,  $T_e$  and  $r$ .  $\dot{m}$  could be written as  $\dot{m} = L_x / (\eta c^2)$  and  $\eta = 10^{-5}$  (Di Matteo et al. 2003).  $r$  is taken as  $50R_{\text{Sch}}$  where the accretion flow emits the detectable X-ray (Manmoto et al. 1997). Then we adjust  $T_e$  to produce observed  $\Gamma$  and  $\dot{m}$ . We found that the  $T_e$  is from  $2.5 \times 10^9$  K to  $3.5 \times 10^9$  K. Such  $T_e$  is consistent with the requirements of the ADAF model (Narayan & Yi 1994).

The light curve modelled by clumpy accretion is consistent well with that observed in M87's nucleus. But such light curve could also be explained by injection/acceleration of high energy particles. Harris et al. (2003) suggests that the above process could produce year-scale X-ray variations observed in HST-1. Following this scheme, when the new energetic electrons is injected or accelerated, the X-ray emission brightens up and the spectra become harder. And then, the X-ray emission decreases by radiative cooling or adiabatic expansion.

A way to differentiate the above mechanisms may be the variability on multi-wavelength. For example, at the picture of particle acceleration, the radio and X-ray emission will both brighten up at the



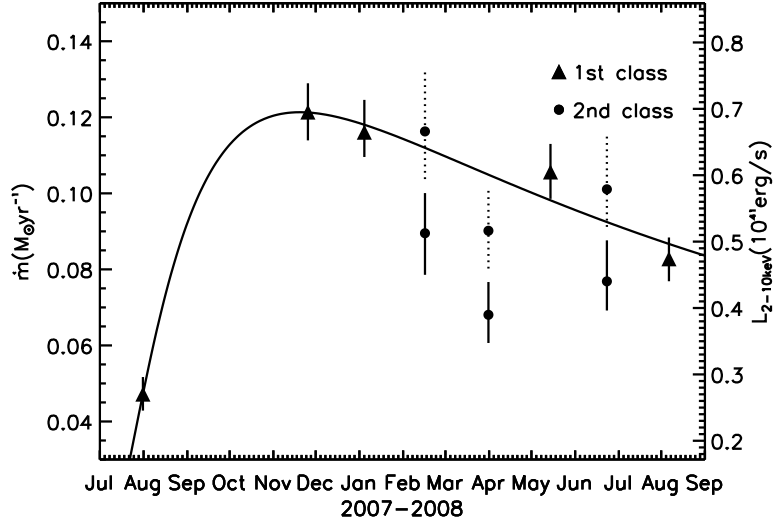


Fig. 5: The evolution of the mass accretion rate for M87’s central blackhole. Triangles: the mass accretion rate/disk X-ray luminosity of the first class; Dots: the mass accretion rate/disk X-ray luminosity of the second class (The disk X-ray luminosity derived with  $\Gamma_1 = 2.1$  is denoted with solid error bars and the disk X-ray luminosity derived with  $\Gamma_1 = 2.0$  is denoted with dash error bars); Solid curve: the fitting result by clumpy accretion model.

same time. Then, at the stage of synchrotron cooling, the radio emission will persist longer than X-ray, because the cooling rate is in proportion to  $E^2$ . However, for the picture of disk evolution, the brightening up at long wavelength (e.g. ultraviolet) should be in advance of that at short wavelength (e.g. X-ray or hard X-ray). To acquire the light curves at multi-wavelength in M87, a long-term joint monitoring from VHE to radio band is being proposed (e.g., Harris et al. 2011 and Raue et al. 2012).

#### 4.2 The X-ray components of flaring state: is the disk influenced by flare?

Our results suggest that the X-ray emission of the second class include both flaring and quiescent components. The spectra of flaring components should be powerlaw-like with lower photon index, for it is most likely emitted through the synchrotron radiation of energetic electrons. In contrast, for quiescent components, we could assume their spectra to be similar to the first class. To decompose these two components, we fit the spectra of the second class with an absorbed double-powerlaw as follows:

$$Model_2 = W_{abs}(n_H) \times (Powerlaw(\Gamma_1, norm_1) + Powerlaw(\Gamma_2, norm_2)), \quad (11)$$

the  $\Gamma_1$  and  $norm_1$  stands for the photon index and normalization of the quiescent component; the  $\Gamma_2$  and  $norm_2$  represent the photon index and normalization of the flaring component.

We fix the  $n_H$  as the  $6.1 \times 10^{20} \text{ cm}^{-2}$ . For the quiescent component, the observations of the first class from 02/2008 to 08/2008 yield a photon index ( $\Gamma_1$ )  $\sim -2.1$ . The photon index of the flaring component ( $\Gamma_2$ ) is hard to be constrained. Here, we consider the coincidence between the VHE and X-ray flare in Feb 2008. The photon index ( $\alpha$ ) of VHE increment is about  $-1.92$  (induced from Albert et al. 2008) and the corresponding X-ray index is  $-1.46$  by  $\Gamma = (\alpha - 1)/2$  as a rough estimation.

In spectra fitting, the photon index is fixed as  $\Gamma_1 = 2.1$  and  $\Gamma_2 = 1.46$ . The derived flux of quiescent component are presented in Fig 5 by dots with solid error bars (Tab 2). Then we also take the  $\Gamma_1 = 2.0$  and  $\Gamma_2 = 1.46$  and the derived flux are shown as the dots with dotted error bars. Our result reveals that the hard X-ray mainly comes from the flaring component and the soft X-ray is dominated by quiescent component (e.g. Fig 6). In three flaring states, the quiescent component only accounts for

Table 2: The result of spectra fitting with absorbed double powerlaw ( $\Gamma_1 = 2.1$  and  $\Gamma_2 = 1.46$ ). The error bars are calculated with the confidence of 68%

ObsID	Quiescent content $10^{40}$ erg/s	Flaring content $10^{40}$ erg/s	$\chi^2/\text{DOF}$
8577	$5.1 \pm 0.6$	$15.1 \pm 1.3$	64.99/65
8578	$3.8 \pm 0.5$	$7.5 \pm 1.0$	53.66/46
8580	$4.4 \pm 0.6$	$10.1 \pm 1.3$	61.16/55

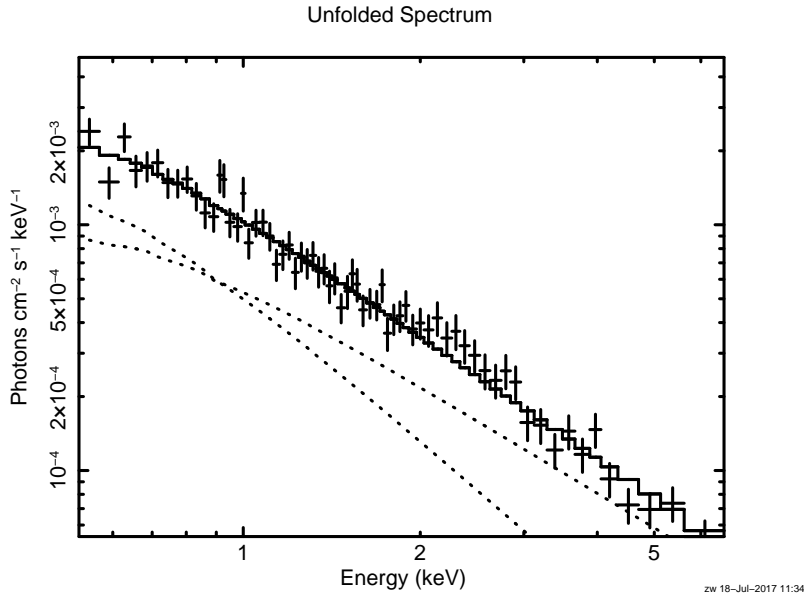


Fig. 6: The unfold spectra of M87's nucleus at flaring state (observation ID:8577, Reduced  $\chi^2 = 0.9998$ ).

the 25% ~ 40% of the X-ray emission. The 2008 Feb.'s flare has the strongest flaring component almost twice as bright as the others', in which a VHE flare was observed by MAGIC and VERITAS (Albert et al. 2008, Acciari et al. 2009). For outbursts occurring in Feb. and Jun. of 2008, the flux of quiescent components is close to the prediction of year-scale evolution ( $< 2\sigma$ ) and it is lower in Apr. 2008.

To check the quiescent component in Apr 2008, in spectra fitting, we fix  $n_H = 6.1 \times 10^{20} \text{ cm}^{-2}$ ,  $\Gamma_1 = 2.1$  and  $\text{norm}_1 = 6.63 \times 10^{-4}$ , which means that the luminosity of quiescent component matches the curve of the steady evolution. The resulting  $\Gamma_2$ ,  $\text{norm}_2$  and reduced  $\chi^2$  are 1.05,  $1.47 \times 10^{-4}$  and 1.38 respectively. The X-ray photon index of -1.05 is too hard for the flaring component. Its corresponding index of the electron's energy spectrum is about -1 ( $\alpha = 2\Gamma + 1$ ), which is far beyond the known accelerating mechanisms and difficult to be explained by current models, such as Fermi acceleration (Lieberman & Lichtenberg 1972) or stochastic acceleration (Fan et al. 2010). Even in the case of  $\Gamma_1 = 2.0$ , the derived luminosity in Apr. of 2008 is still lower than the others. So it is possible that the flux of quiescent component in Apr. 2008 could not reach the value of year-scale evolution. The mechanism for such a phenomenon is unclear. One possibility is that the disk was disturbed by outburst if the flare occurred in the ADAF near the black hole.

Our analysis reveals two kinds of variations for nuclear X-ray emission: a year-scale variation and a month-scale variation. The year-scale variation may come from the evolution of ADAF disk. And the month-scale variation may be produced by the mini-jet. So the process of jet-in-disk is favored for explaining the variations of M87's nucleus. The mini-jet may be produced by the re-connection of the magnetic field (Giannios et al. 2010). When magnetic re-connection occurs, the local electrons in ADAF

disk will be accelerated to high energy. Correspondingly, X-ray spectra change from the first class to the second class: the flaring component brightens up and the quiescent component declines, as revealed in *Chandra* observation. Above process can only happen in the magnetically arrested disk, which could be investigated in the future by polarization detection.

## 5 CONCLUSIONS

In this paper, we re-analyze the M87's nuclear spectra of 8 *Chandra* observations from 2007 to 2008 and discover a year-scale variation of the disk emission. Then we discuss the evolution of accretion disk based on this year-scale variation. At last, we also try to decompose the spectra of the flaring states.

The conclusion are listed as follows:

1. We obtain both the month-scale and year-scale variations in X-ray light curve of M87's nucleus. The month-scale variation is produced by X-ray flares. The year-scale variation originates from the evolution of accretion disk. Such a disk evolution could be explained well by the accretion of a gas ring, which might result from a tidal disrupted cloud of  $\sim 0.5 M_{\odot}$ .

2. The X-ray spectra of M87's nucleus could be divided into two classes: 'quiescent state' and 'flaring state'. The ADAF component likely dominates the quiescent state. At flaring state, the X-ray emission of nucleus includes both the ADAF component and 'flaring component', where the ADAF component accounts for  $\sim 30\%$ . But this fraction strongly depends on the assumed photon indexes. More accurate observations are needed to constrain the results.

3. In flaring state, the ADAF component probably matches the value of year-scale evolution. But in observation of Apr. 2008, the ADAF component shows the trend of sharp decreasing, suggesting that accretion flow was disturbed by the outburst occurring in the ADAF of M87.

## ACKNOWLEDGEMENTS

This work is supported by the CASSACA Postdoc Grant (from the Chinese Academy of Sciences, CAS), the Visiting Scholarship Grant (administered by the CAS South America Center for Astronomy, CASSACA, NAO), Science & Technology Department of Yunnan Province - Yunnan University Joint Funding (2019FY003005) and National Science Foundation of China (grant 11203019, 11863006).

Cheng Cheng is supported by the Young Researcher Grant of National Astronomical Observatories, Chinese Academy of Science and the National Natural Science Foundation of China, No. 11803044. This work is sponsored (in part) by the Chinese Academy of Sciences (CAS), through a grant to the CAS South America Center for Astronomy (CASSACA).

## References

- Abramowski, A., Acero, F., Aharonian, F., et al. 2012, *ApJ*, 746, 151  
 Acciari, V. A., Aliu, E., Arlen, T., et al. 2009, *Science*, 325, 444  
 Adams, S. C., Perlman, E. S., & Cara, M. 2012, *Journal of the Southeastern Association for Research in Astronomy*, 5, 12  
 Albert, J., Aliu, E., Anderhub, H., et al. 2008, *ApJ*, 685, L23  
 Aliu, E., Arlen, T., Aune, T., et al. 2012, *ApJ*, 746, 141  
 Arnaud, K. A. 1996, *Astronomical Data Analysis Software and Systems V*, 101, 17  
 Biretta, J. A., Zhou, F., & Owen, F. N. 1995, *ApJ*, 447, 582  
 Boksenberg, A., Macchetto, F., Albrecht, R., et al. 1992, *A&A*, 261, 393  
 Cui, Y.-D., Yuan, Y.-F., Li, Y.-R., & Wang, J.-M. 2012, *ApJ*, 746, 177  
 Davis, J. E. 2001, *ApJ*, 562, 575  
 Di Matteo, T., Allen, S. W., Fabian, A. C., Wilson, A. S., & Young, A. J. 2003, *ApJ*, 582, 133  
 Elvis, M., Wilkes, B. J., McDowell, J. C., et al. 1994, *ApJS*, 95, 1  
 Fabian, A. C., & Rees, M. J. 1995, *MNRAS*, 277, L55  
 Fan, Z., Liu, S., & Fryer, C. L. 2010, *MNRAS*, 406, 1337

- Frank, J., King, A., & Raine, D. J. 2002, *Accretion Power in Astrophysics*, by Juhan Frank and Andrew King and Derek Raine, pp. 398. ISBN 0521620538. Cambridge, UK: Cambridge University Press, February 2002., 398
- Giannios, D., Uzdensky, D. A., & Begelman, M. C. 2010, *MNRAS*, 402, 1649
- Gu, M., & Cao, X. 2009, *MNRAS*, 399, 349
- Hada, K., Kino, M., Nagai, H., et al. 2012, *ApJ*, 760, 52
- Harris, D. E., Biretta, J. A., Junor, W., et al. 2003, *ApJ*, 586, L41
- Harris, D. E., Cheung, C. C., Biretta, J. A., et al. 2006, *ApJ*, 640, 211
- Harris, D. E., Cheung, C. C., Stawarz, L., Biretta, J. A., & Perlman, E. S. 2009, *ApJ*, 699, 305
- Harris, D. E., Massaro, F., Cheung, C. C., et al. 2011, *ApJ*, 743, 177
- Hilburn, G., & Liang, E. P. 2012, *ApJ*, 746, 87
- Ho, L. C. 1999, *ApJ*, 516, 672
- Ho, L. C. 2008, *ARA&A*, 46, 475
- Hopkins, P. F., Richards, G. T., & Hernquist, L. 2007, *ApJ*, 654, 731
- Ishibashi, W., & Courvoisier, T. J.-L. 2009, *A&A*, 504, 61
- Li, Y.-R., Yuan, Y.-F., Wang, J.-M., Wang, J.-C., & Zhang, S. 2009, *ApJ*, 699, 513
- Levinson, A., & Rieger, F. 2011, *ApJ*, 730, 123
- Lieberman, M. A., & Lichtenberg, A. J. 1972, *Phys. Rev. A*, 5, 1852
- Lin, D. N. C., & Pringle, J. E. 1987, *ApJ*, 320, L87
- Manmoto, T., Mineshige, S., & Kusunose, M. 1997, *ApJ*, 489, 791
- Marshall, H. L., Miller, B. P., Davis, D. S., et al. 2002, *ApJ*, 564, 683
- Miller, J. M., Homan, J., & Miniutti, G. 2006, *ApJ*, 652, L113
- Narayan, R., & Yi, I. 1994, *ApJ*, 428, L13
- Nemmen, R. S., Storchi-Bergmann, T., & Eracleous, M. 2014, *MNRAS*, 438, 2804
- Perlman, E. S., Biretta, J. A., Zhou, F., Sparks, W. B., & Macchetto, F. D. 1999, *AJ*, 117, 2185
- Perlman, E. S., Adams, S. C., Cara, M., et al. 2011, *ApJ*, 743, 119
- Pian, E., Romano, P., Maoz, D., et al. 2010, *MNRAS*, 401, 677
- Raue, M., Stawarz, L., Mazin, D., et al. 2012, *International Journal of Modern Physics Conference Series*, 8, 184
- Rybicki G. B. & Lightman A. P. 1979, *Radiative Processes in Astrophysics*. New York: Wiley
- Stark, A. A., Gammie, C. F., Wilson, R. W., et al. 1992, *ApJS*, 79, 77
- Strubbe, L. E., & Quataert, E. 2009, *MNRAS*, 400, 2070
- Wang, J.-M., Li, Y.-R., Wang, J.-C., & Zhang, S. 2008, *ApJ*, 676, L109
- Wang, J.-M., Cheng, C., & Li, Y.-R. 2012, *ApJ*, 748, 147
- Wilson, A. S., & Yang, Y. 2002, *ApJ*, 568, 133
- Wu, Q., Yuan, F., & Cao, X. 2007, *ApJ*, 669, 96
- Yuan, F. 2003, *ApJ*, 594, L99
- Yuan, F., Taam, R. E., Misra, R., Wu, X.-B., & Xue, Y. 2007, *ApJ*, 658, 282
- Yuan, F., & Narayan, R. 2014, *ARA&A*, 52, 529